ACS APPLIED MATERIALS & INTERFACES

Research Article

www.acsami.org

Highly Efficient Wettability Control via Three-Dimensional (3D) Suspension of Titania Nanoparticles in Polystyrene Nanofibers

Min Wook Lee, Seongpil An, Bhavana Joshi, Sanjay S. Latthe, and Sam S. Yoon*

School of Mechanical Engineering, Korea University, Anam-dong Seongbuk-gu, Seoul, Korea

ABSTRACT: Electrospinning is a simple and highly versatile method for the large-scale fabrication of polymeric nanofibers. Additives or fillers can also be used to functionalize the nanofibers for use in specific applications. Herein, we demonstrate a novel and efficient way to fabricate superhydrophobic to hydrophilic tunable mats with the combined use of electrospinning and electrospraying that may be suitable for mass production on the merits of rapid deposition. The tunable nanocomposite mats were comprised of hydrophobic polystyrene nanofibers and hydrophilic titania nanoparticles. When the electrical conductivity of the electrospinning solution was increased, the surface morphology of the mats changed noticeably from a bead-on-string structure to an almost bead-free structure. Polystyrene (PS)−titania nanocomposite mats initially yielded a static water contact angle as high as 140° ± 3°. Subsequently exposing these mats with relatively weak ultraviolet irradiation (λ = 365 nm, I = 0.6 mW/cm^2) for 2 h, the unique 3D suspension of the photoactive titania nanoparticles maximized the hydrophilic performance of the mats, reducing the static water contact angle to as low as 26° ± 2°. The tunable mats were characterized by scanning electron microscopy (SEM), static water contact angle (WCA) measurements, and energy-dispersive X-ray spectroscopy (EDX). Our findings confirmed that the tunable mats fabricated by the simultaneous implementation of electrospraying and electrospinning had the most efficient ultraviolet (UV)-driven wettability control in terms of cost-effectiveness. Well-controlled tunable hydrophobic and hydrophilic mats find potential applications in functional textiles, environmental membranes, biological sensors, scaffolds, and transport media.

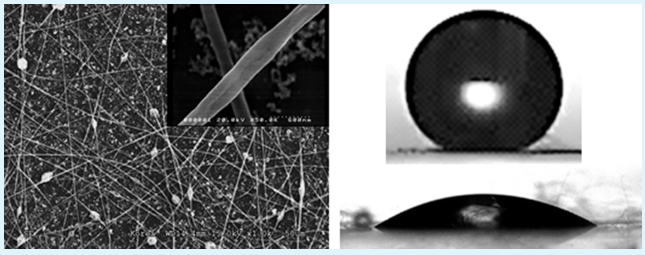

KEYWORDS: *wettability, electrospinning, electrospray, polystyrene nanofibers, titania nanoparticles, 3D suspension*

1. INTRODUCTION

Electrospinning is a simple, versatile, and cost-effective technique for fabricating extremely long electrostatic polymer fibers with diameters ranging from 2 nm to several micrometers, utilizing electrical forces.[1,2] Electrospun films consisting of a continuous, nonwoven web of nanofibers usually have high surface area-to-volume ratio, complex pore structure, and unique physical and mechanical properties.[3] A recent review article[4] thoroughly summarized the electrospinning fabrication of fibers from various polymeric materials. It correlated various parameters, including the concentrations of the polymers, the solvents, and the different instrument setups, and also discussed the theory of superhydrophobicity and self-cleaning. Solid−liquid interfacial energy can be minimized by modifying surface chemistry as well as surface roughness.[5] Understanding the complementary roles of surface energy and surface roughness of natural nonwetting surfaces including numerous plant leaves especially lotus leaves,[6] legs of the water strider,[7] and duck feathers[8] has led to the development of several biomimetic superhydrophobic surfaces, which exhibit static water contact angles of >150° and lower roll-off angles. Among these, smart surfaces with switchable wettability between superhydrophobicity and superhydrophilicity have received much attention for numerous industrial applications. Wetting properties can be engineered to external stimuli such as light irradiation, pH changes, solvent exposure, electrical potential, magnetic field, mechanical force, or temperature.[9−11] Among the methods used to control surface wettability, light switching has received great attention, because of its rapid controllability. Such wettability tuning is important for a wide range of applications including low-drag surface modification, material protection, water and air filters, water harvesting, and biomedical films.[12−14] For example, high water adsorption (hydrophilicity) is needed for water purification mats and high water repellency (hydrophobicity) for protection of biomaterials from corrosion or infection. Convenience could be best served by a material with both properties of hydrophilicity and hydrophobicity. A three-dimensional (3D) structured tunable mat can be used for applications that require both features of hydrophilicity and hydrophobicity, such as functional textiles, environmental membranes, biological sensors, scaffolds, and transport media.[15−17]

Recently, synthesis of organic−inorganic hybrid materials has received much attention in material science. Using composite materials made from the combination of nanosized inorganic and organic materials can provide advantages over the use of a

Received: September 23, 2012
Accepted: January 24, 2013
Published: January 24, 2013

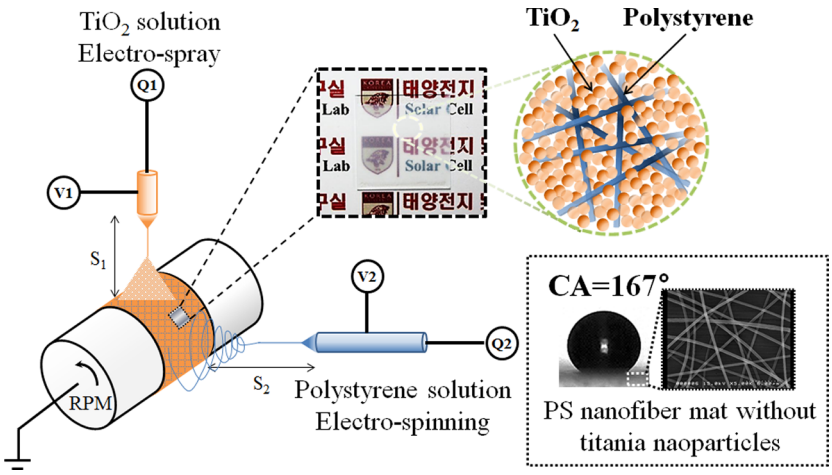

Figure 1. Fabrication of titania-decorated nanofiber mat via electrospinning polymer solution and electrospraying titania nanoparticles. In the experiments, the nozzle-to-substrate distances are S_1 = 2 cm and S_2 = 12 cm; V_1 and V_2 are the applied voltage; and Q_1 and Q_2 indicate flow rates for electrospraying and electrospinning, respectively.

single organic or inorganic material. The incorporation of a small amount of inorganic nanoparticles, such as titania and zinc oxide, can improve the wetting, mechanical, thermal, optical, antimicrobial, antifouling and catalytic properties of a polymer matrix.[18] Various functional materials can be deposited by physical vapor deposition (PVD) and chemical vapor deposition (CVD).[19] Surface modification processes, such as post-annealing,[20] and chemical and plasma etching,[21,22] have been applied to improve the hydrophilicity and/or hydrophobicity of functional films. However, these deposition processes and surface modification procedures are often technically complicated, time-consuming, high energy-consuming, and thus not economically viable. An alternative would be electrospinning, which is a simple and cost-effective technique for producing functional mats or membranes whose fiber diameters range from a few nanometers to micrometers.[1,2] Specifications of a mat, such as fiber size, porosity, and morphology, can be controlled by process parameters, such as deposition time, applied voltage, and nozzle-to-collector distance,[23−25] and by material properties such as polymer concentration and solvent evaporation rate,[26−28] etc. The outstanding properties and multifunctionality of these mats make them a promising candidate for applications in tissue engineering,[29,30] dye-sensitized solar cells electrodes,[31] microarrays,[32] films and membrane fabrication,[33] textiles,[34] fuel cells,[35] and water purification filters.[36]

In the present work, a superhydrophobic mat with a highly porous surface structure was obtained from a material of low surface energy, such as polystyrene (PS). Polystyrene is a hydrophobic, atmosphere-stable, dielectric, and electrospinable polymer, which has long been used to prepare superhydrophobic surfaces via electrospinning.[37] To make the mat tunable, hydrophilic material such as titania was electrosprayed onto the functional mat simultaneously. We chose titania as the working material to obtain the tunable feature of hydrophilicity[38] because titania is inexpensive and abundant, chemically inert, non-photodegradable, nontoxic, photoinducible by sunlight, manufacturable under atmospheric conditions, and environmentally friendly. Hydrophilicity is achieved when photosensitive titania is exposed to ultraviolet (UV) light; photogenerated holes react with (absorbed) water to produce OH^- radicals. This reaction also produces Ti^{3+} and oxygen vacancies, which, in turn, adsorb water molecules at the defect sites to further promote hydrophilicity. On the other hand, superhydrophobic surfaces of PS mats with static water contact angles (WCAs) ranging from 143.8° to 159.5° were reported by Miyauchi et al.[28] However, their electrospun mats did not have the tunable feature of hydrophilicity. Asmatulu et al.[39] reported electrospun mats decorated with titania nanoparticles which showed superhydrophobicity. However, the WCA range of their mats was quite limited to ΔWCA < 60°, which can be improved by properly controlling the process parameters. In our electrospun mats fabricated by the new method, the WCA reached as high as 140° ± 3° and after exposing the mats for 2 h to relatively weak UV irradiation (λ = 365 nm, I = 0.6 mW/cm^2), WCA dramatically reduced to 26° ± 2°. The process parameters that yielded the highest range of ΔWCA (∼115°) were identified. Our unique installation of electrospun PS nanofibers and electrosprayed titania nanoparticles yielded a truly 3D structured PS−titania nanocomposite mat, which showed UV-driven superhydrophobic-to-hydrophilic conversion. The goal of this work is to show the high performance, yet easy fabrication, of a 3D tunable mat consisting of PS nanofibers and titania nanoparticles.

2. EXPERIMENTAL SECTION

The fabrication process of a titania-incorporated PS nanofiber mat is shown in Figure 1. Titania nanoparticles (P25, Daegusa, Germany) are a mixture of 80% anatase and 20% rutile, which are dispersed in ethanol solution to facilitate their electrospray deposition onto glass substrates attached to a cylinder rotating at 100−500 rpm. The amount of titania nanoparticles was purposely set low (0.3 wt %) to prevent precipitation and aggregation of the particles as much as possible. No special dispersant was used. Titania nanoparticles were electrosprayed, starting from the top of the cylinder, while the nanofibers were electrospun from the side for 5−15 min (cf. Figure 1).

Polystyrene solution (M_w = 192 000, Sigma−Aldrich, 20 wt % PS pellet dissolved in dimethylformamide, DMF) was horizontally electrospun onto a rotating cylinder to produce nanofibers. A few drops of nitric acid were added to the polystyrene solution to promote the solution's electrical conductivity without changing the solution's viscosity and surface tension. High-strength PS nanofibers were used to firmly hold the sprayed titania nanoparticles. The mass percentage of the TiO_2 particles in the nanocomposite mat was ∼22.3%, considering the mass of TiO_2 and PS is 2.49 and 8.7 g per unit area deposited, respectively.

Nozzles used for both electrospraying and electrospinning had diameters of 4 mm and 0.25 mm, respectively. In electrospraying (noted with $(\ )_1$) and electrospinning (noted with $(\ )_2$), dc voltages of V_1 = 7 kV and V_2 = 9 kV were applied at flow rates of Q_1 = 1 mL/h and Q_2 = 0.2 mL/h, respectively (see Figure 1). The nozzle-to-substrate distances (S_1 and S_2), which are important process parameters, were optimized to S_1 = 2 cm and S_2 = 12 cm, respectively, to yield uniform distributions of the nanoparticles, which minimized the agglomeration of the titania nanoparticles. The microstructures of the titania-incorporated nanofiber mats were characterized by high-resolution scanning electron microscopy (Hitachi, Model S-5000). The average fiber diameter and the size of the beads were calculated from SEM images. About 100 fibers and 50 beads were collected to estimate the fiber diameter and the size of the beads. The tunable wettability of the mats was determined by static water contact angle (WCA) measurements under relatively weak UV light irradiation (I = 0.6 mW/cm^2, λ = 365 nm) in an open air environment. All samples were kept inside a dark box for 24 h prior to any UV light illumination test. The maximum UV light illumination time was t_{UV} = 120 min. The average contact angle value was adopted as the indicator of wettability by measuring contact angles at five fresh positions on the same sample.

Regarding the contact angle measurement, all electrospun mats were kept inside a dark box for two days prior to the contact angle measurement. Then each mat was illuminated inside a UV light box for various durations. Afterward, the mat was taken outside the UV box and then an ultrapure water droplet (20 MΩ resistivity at 20 °C) 2 mm in diameter was placed on the film for a snapshot. The time interval between when a mat were taken out of the UV box and when the photosnapshot was taken was set to 1 min, to minimize the effect of the surrounding indoor lights. For increase data reliability, the average result of three repeated tests was taken as the final contact angle value.

The chemical compositions of the mats were investigated by energy-dispersive X-ray spectroscopy (EDX) (Horiba, Model EX-200). Carbon content was assumed to represent the amount of PS. The electrical conductivities of the all spinning solutions were measured using a conductivity meter (Model HI-98360, HANNA Instruments, USA). The test for each case was repeated three times to ensure repeatability. All of the electrospun mats from this study were fabricated with deposition times of 15 min or less without any further post-treatment.

3. RESULTS AND DISCUSSION

We observed that the changes in electrical conductivity of the spinning solution determined the final morphology of the PS nanofibers to yield either bead-on-string or bead-free nanofibers. The photoinduced activity of the titania nanoparticles contributed to the mat's hydrophilicity under UV exposure, while the chemical property and porosity of the electrospun PS nanofibers contributed to the mat's hydrophobicity. PS−titania nanocomposite mats initially provided hydrophobicity because of the 3D structure of the nanofibers, whose PS itself had low surface energy. Upon UV exposure, the photoinduced hydrophilicity of the titania nanoparticles dominated[40] over the hydrophobicity of the nanofibers. Thus, these materials (i.e., titania and PS) were the sources of two competing mechanisms inside the tunable mats.

3.1. Surface Morphology of PS−Titania Nanocomposite Mats. In general, the surface of a mat can be modified by controlling process parameters such as the precursor's thermophysical properties and the operating conditions. The process parameters determine the appearance or disappearance of bead-on-string or bead-free nanofibers. The electrical conductivity of the spinning precursor greatly affected the bead formation along the nanofibers. When the spinning solution has low electrical conductivity, capillary-driven instability dominates, resulting in the formation of beads on

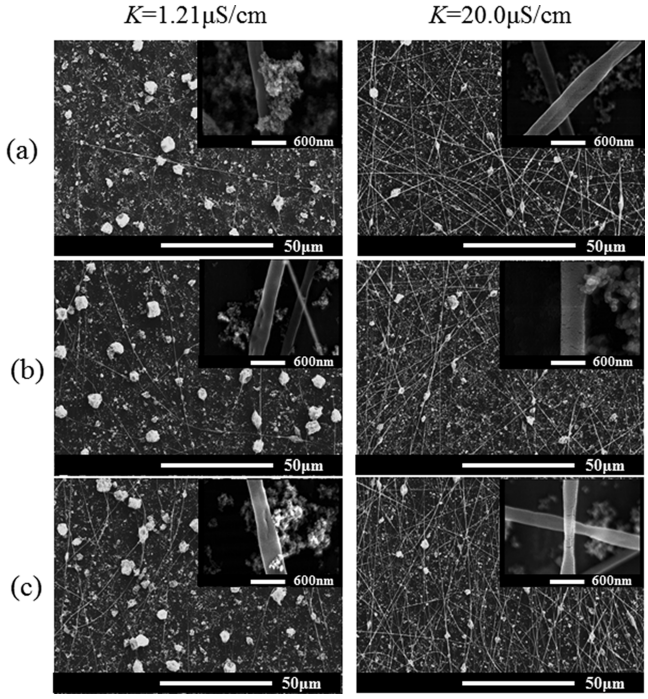

Figure 2. Effect of drum rotation speed, shown using SEM images of PS−titania composite film: (a) 100 rpm, (b) 300 rpm, and (c) 500 rpm (t_{dep} = 5 min).

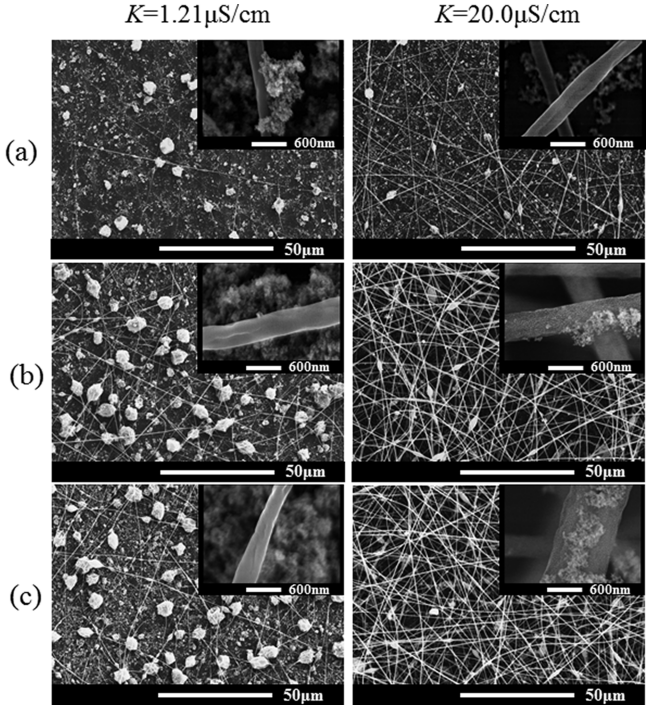

Figure 3. Effect of deposition time, shown using SEM images of PS nanofibers and titania nanoparticles: (a) t_{dep} = 5 min, (b) t_{dep} = 10 min, and (c) t_{dep} = 15 min (100 rpm).

nanofibers.[41,42] When the polymer solution has higher electrical conductivity, more charges are delivered to the surface of the spinning fiber. In general, charges smoothly elongate the jet or fiber under the influence of an electric field. Therefore, it seems natural that more-uniform fibers with less beads are formed with increasing electrical conductivity of the spinning solution,

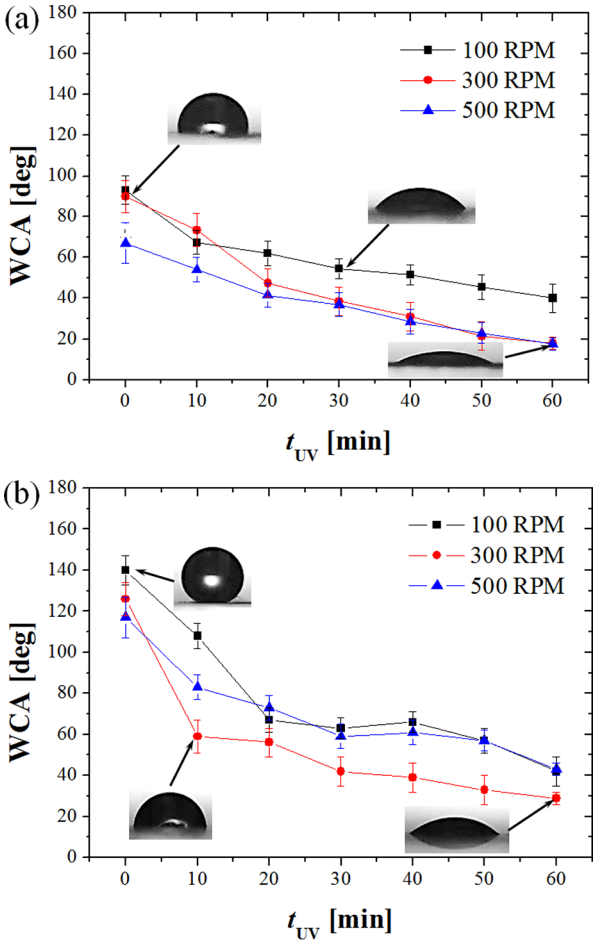

Figure 4. Water contact angle (WCA) of the mat, as a function of UV light illumination time, for various cylinder rotation speeds. (t_{dep} = 5 min): (a) K = 1.21 μS/cm (WCA = 97° for PS nanofiber mat) and (b) K = 20.0 μS/cm (WCA = 167° for PS nanofiber mat).

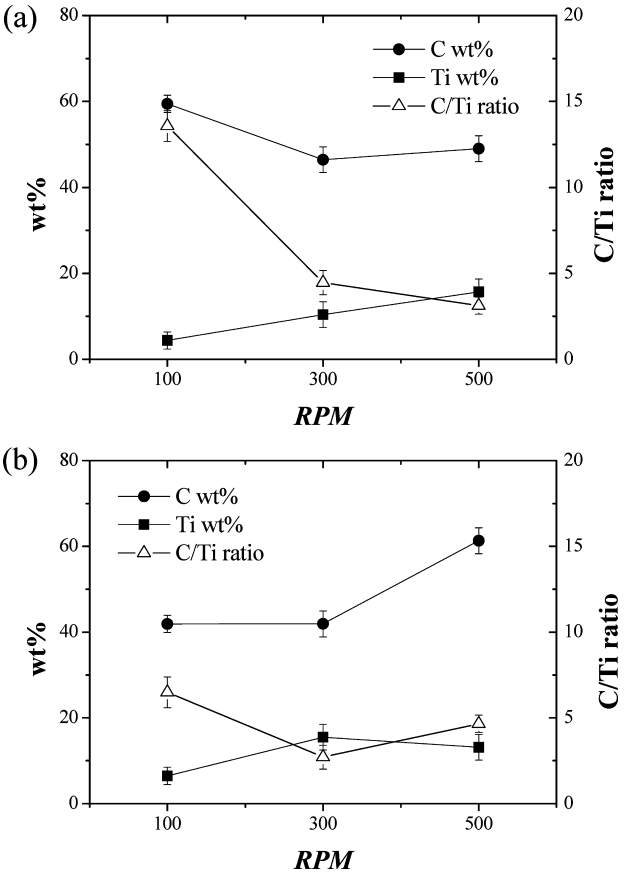

Figure 5. Effect of cylinder rotation speed on the weight percent ratio of polystyrene to titania: (a) K = 1.21 μS/cm and (b) K = 20.0 μS/cm (t_{dep} = 5 min).

as shown in Figure 2. The microstructural images of PS−titania nanocomposite mats obtained at different electrical conductivities (i.e., K = 1.21 and 20.0 μS/cm) and various cylinder rotating speeds (i.e., 100, 300, and 500 rpm) at fixed deposition time (t_{dep} = 5 min) are shown in Figure 2.

The surface morphology changed from the bead-on-string to nearly bead-free nanofibers when the conductivity of the spinning solution increased. The number and size of the beads were greatly reduced when the electrical conductivity increased. In both low and high electrical conductivity cases of the spinning solution, aggregates of titania nanoparticles were entrapped in the pores of the PS nanofibers; see insets of Figure 2a−c. Some titania nanoparticles were physically attached onto the peripheries or surfaces of the PS nanofibers.

For the lower electrical conductivity (K = 1.21 μS/cm) of the spinning solution, bead-on-string nanofibers were observed. The bead size ranged from 4 μm to 5 μm, and the nanofiber diameter ranged from 250 nm to 350 nm for all drum rotation speeds (Figure 2, left column). When the electrical conductivity of the spinning solution was increased to 20.0 μS/cm, most of the beads were removed at all drum rotation speeds (compare the left and right images in Figure 2). In addition, the number density and the diameter of the nanofibers had also markedly increased. Nanofibers with diameters in the range of 400−550 nm and few beads were observed (see the right column in Figure 2). The columnar jet of the highly conductive polymeric solution was stretched due to the repulsion of the excessive charges distributed on the jet surface, thereby preventing capillary instability, which would have formed beads. Thus, increased conductivity of the spinning solution produces bead-free fibers that are uniform and thin.[43,44] Uyar and Besenbacher[45] also reported the formation of bead-free fibers with the use of PS in DMF solution whose electrical conductivity was varied from 1.1 μS/cm to 7.3 μS/cm. In our case, the higher electrical conductivity (K = 20.0 μS/cm) of the spinning solution increased the charge density of the polymer solution, and this charge density increase led to greater repulsion and greater bending instability during electrospinning; as a result, the electrospun fibers were stretched into thinner fibers and the beads were nearly eliminated.

A drum rotation speed did not seem to have prominent influence on surface morphology, as depicted in Figure 2. However, Figure 3 shows that deposition time (t_{dep}) did have a prominent influence on surface morphology since more beads and nanofibers were deposited onto the substrate with increasing t_{dep}. For the lower electrical conductivity (K = 1.21 μS/cm) of the spinning solution, the number density of the beads and nanofibers, of course, increased as t_{dep} increased from 5 min to 15 min at a fixed 100 rpm. The bead size (4−5 μm), and the fiber diameter (250−350 nm) remained nearly the same with increasing t_{dep}, because they are controlled by the electrical conductivity of the spinning solution. However, for the high electrical conductivity (K = 20.0 μS/cm) case, the beads disappeared and nearly bead-free nanofibers (diameter in

dx.doi.org/10.1021/am303008s | ACS Appl. Mater. Interfaces 2013, 5, 1232−1239

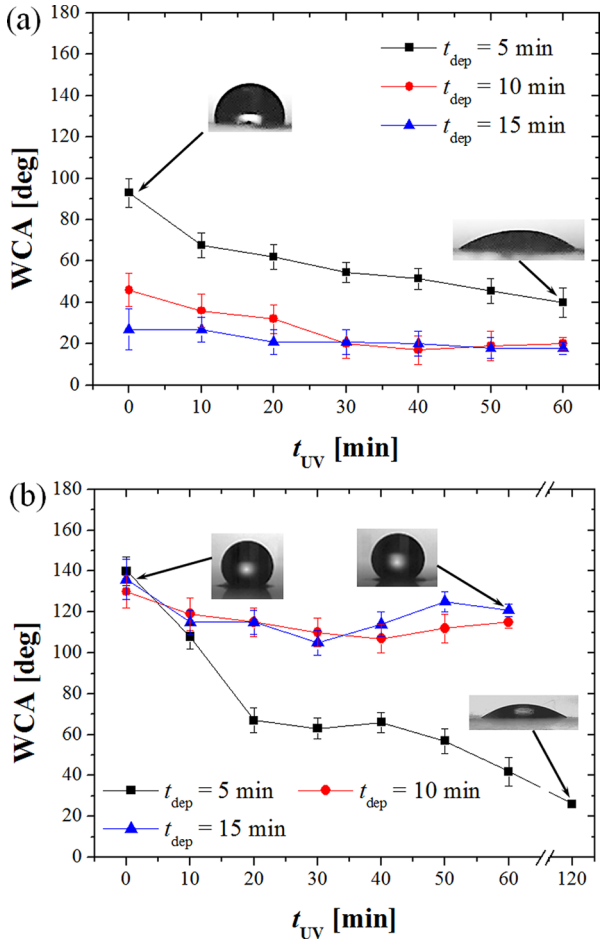

Figure 6. Water contact angle (WCA) of the mat, as a function of UV light illumination time (t_{UV}), for various t_{dep} (100 rpm): (a) K = 1.21 μS/cm (WCA = 97° for PS nanofiber mat) and (b) K = 20.0 μS/cm (WCA = 167° for PS nanofiber mat).

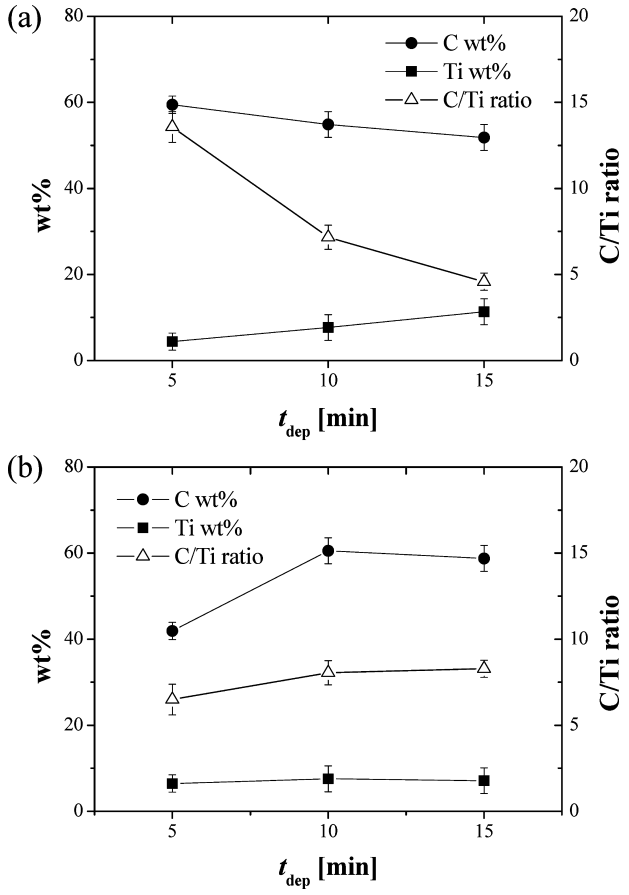

Figure 7. Effect of deposition time on the weight percent ratio of polystyrene to titania: (a) K = 1.21 μS/cm and (b) K = 20.0 μS/cm (100 rpm).

the range of 400−850 nm) were obtained. The number density of the nanofibers increased as t_{dep} increased. More nanofibers may not be desirable for tuning of hydrophobicity and hydrophilicity as they may hinder the photoinduced activity of the titania nanoparticles. Figure 3 also shows that the titania nanoparticles were entrapped in the pores and they were physically adsorbed onto the PS nanofibers for all deposition times (5 min ≤ t_{dep} ≤ 15 min).

3.2. Effect of Drum Rotation Speed and UV Irradiation on WCA. Water contact angle (WCA) is a common measure of hydrophobicity. The WCA strongly depends on surface chemical composition, as well as surface roughness. Figure 4 compares the WCA of a PS−titania nanocomposite mat for various drum rotation speeds (100, 300, and 500 rpm) and fixed deposition time (t_{dep} = 5 min) and the change of WCA for different UV irradiation time (t_{UV}). The effect of electrical conductivity (the effect of bead-on-string or bead-free nanofiber structure on WCA) is shown in the comparison between Figure 4a and 4b.

Thinner fibers and higher number densities of beads improve superhydrophobicity,[46] because of the air pockets densely populated between the beads, which lead to water drops in the Cassie−Baxter state. Even though the beaded fibers promote superhydrophobicity, in practice, they are not desirable because of their poor mechanical properties, such as their yield and adhesion strength. In general, nanofibers without beads are less hydrophobic and lead to low WCAs or very large roll-off angles,[47] as compared to nanofibers with beads. Efforts have been made to maintain both superhydrophobicity and superior mechanical strength by modifying the surface structure.[48]

It is still a challenge to produce a bead-free superhydrophobic nanofiber mat or a bead-free membrane having a high WCA and a low roll-off angle. We aim to overcome this challenge in this study. The bead-on-string PS nanofiber structure that resulted from the low electrical conductivity (K = 1.21 μS/cm) of the spinning solution without titania nanoparticles showed a WCA of ~97° ± 3°, whereas the bead-free PS nanofiber structure from the high electrical conductivity (K = 20.0 μS/cm) of the spinning solution without titania nanoparticles showed WCA ≈ 167° ± 2° (see an inset in Figure 1). In the bead-on-string nanofiber structure, irregularly sized beads were randomly distributed in low density.[49] As a result, the air pockets between the beads were too sparse and not uniform; thus, the ideal Cassie−Baxter hydrophobic state could not be realized. Instead, these sparse and nonuniform air pockets operate to absorb water, thereby resulting in the Wenzel state of a moderate water contact angle of WCA ≈ 97° ± 3°, which was slightly higher than that of the spin-coated smooth PS film (~93°) in ref 49. Conversely, a surface of "bead-free" nanofiber structure maintained the air pockets between uniform nanofibers, resulting in the Cassie−Baxter state. If sufficient beads had been formed, it would also have resulted in superhydrophobicity, just as other previous studies had shown.[46]

dx.doi.org/10.1021/am303008s | ACS Appl. Mater. Interfaces 2013, 5, 1232−1239

Table 1. Comparisons for the Fabrication Methods and Their WCA Tunability Performance

	method	fabrication material[a]	time	WCA	t_{UV} (min)	UV intensity (W/cm^2)
Lee et al.[54]	MOCVD	TiO_2	NA[b]	75° → 0°	100	10
Zhang et al.[55]	dip coating and plasma etching	TiO_2 (ODP-modified)	>2 days	166° → 0°	240	1.0
Jin et al.[40]	UV/ozone treatment and liquid-phase deposition	TiO_2	8 h	130° → 10°	180	25
present	electrospraying and electrospinning	TiO_2 and PS fiber	5 min	140° → 26°	120	0.6

[a]ODP = octadecylphosphonic acid; PS = polystyrene. [b]NA = not available.

However, our bead-free superhydrophobic mat is preferred to the "bead-sufficient" superhydrophobic mat, with respect to mechanical stability and reliability.

In the previous section, the PS−titania composite mat that was fabricated from the spinning solution of the lower electrical conductivity (K = 1.21 μS/cm) was comprised of numerous beads, because of strong capillary instability. These "poorly populated" beads work against hydrophobicity and has a strong influence on WCA, as shown in Figure 4a; the initial WCA values (t_{UV} = 0) remain in the range of 67° < WCA < 93° for all cylinder rotation speeds. However, at the higher electrical conductivity (see Figure 4b for K = 20.0 μS/cm), the initial WCA values (t_{UV} = 0) lie in the range of 117° < WCA < 140° for all cylinder rotation speeds.

At the higher electrical conductivity, the nanofibers were more uniform with few beads; this promoted hydrophobicity, because of the air trapped between the uniform pores and the increased interfacial area between the PS−titania composite mat and a water drop. At the lower electrical conductivity, the bulk of PS materials was consumed to form beads rather than cylindrical nanofibers, so the interfacial area was reduced.

The equilibrium WCA (∼167° ± 2°, the nanofiber comprised of PS only) had dramatically decreased to ∼140° ± 3° after incorporating the titania nanoparticles in the PS nanofiber matrix; this decrease indicated a transient from the stable to the metastable Cassie−Baxter state. Titania nanoparticles are hydrophilic in nature, even without UV.[50] They can physically and chemically absorb water molecules to reduce WCA.

Contact angle variation is critical in increasing applications that utilize superhydrophobicity or superhydrophilicity. We measured the contact angle variation with time to characterize the durability of our coating.[51−53] To analyze the deterioration of the hydrophobic state, we used deionized water as the test liquid. The total time necessary for equilibrating the initial shape of a water drop on a surface did not exceed milliseconds, which is herein referred to as the "initial wetting angle", which we measured to be within 2 s after the deposition of the water drop. The error of WCA measurement was within ±1° for all angles measured on the surface. The PS nanofiber retained its superhydrophobicity for (∼167° ± 2°) more than 24 h. On the other hand, the WCA on the PS−titania nanocomposite surface decreased gradually from 140° ± 3° to 28° ± 1° after 10 h of continuous contact with water and it remained at 28° ± 1°. In the latter case, the gradual decrease in WCA was due to the slow but steady interaction of the water molecules with the physically adsorbed titania nanoparticles on and inside the PS nanofiber matrix.

As the UV light exposure time (t_{UV}) was increased, photoinduced hydrophilicity occurred, because of the entrapped titania nanoparticles in the PS nanofiber matrix and, thus, WCA was reduced for all cases. In the comparison between Figures 4a and 4b, it is observed that the PS−titania composite mats fabricated at the higher electrical conductivity of the spinning solution provide larger ΔWCAs (which is the absolute WCA difference between t_{UV} = 0 and t_{UV} = 60 min), which allowed more tunability between hydrophilicity and hydrophobicity. In the case of the PS−titania composite mats fabricated at K = 1.21 μS/cm, the largest ΔWCA (∼72° ± 4°) was obtained at 300 rpm (Figure 4a). In Figure 4b, the composite mats fabricated at K = 20 μS/cm showed the largest ΔWCA (∼101° ± 3°) at 300 rpm, which was thus considered optimal. Also, the sharpest WCA change was observed for the 300 rpm case; this mat became more quickly hydrophilic than the others, indicating a relatively larger content of titania nanoparticles.

To confirm the larger content of titania nanoparticles for the 300 rpm case, we measured the atomic weight percentages of carbon (which is an indication of nanofiber amount) and titanium (which is an indication of titania amount), using energy-dispersive X-ray spectroscopy (EDX). Figure 5 compares the weight percentages of carbon and titanium. For K = 20.0 μS/cm (which corresponds to Figure 4b with few beads), the relative titanium amount is the largest, as expected. For K = 1.21 μS/cm (which corresponds to Figure 4a with numerous beads), the smallest WCA is seen for the 500 rpm case, while the largest ΔWCA is seen for the 300 rpm case. Thus, the titanium amount is the largest at 500 rpm, as also confirmed by the EDX data from Figure 5.

3.3. Effect of t_{dep} and Beads on WCA. With increasing deposition time (t_{dep}), more PS nanofibers and titania nanoparticles were deposited. It is natural to assume that large amounts of both materials would enhance the tunability between hydrophobicity and hydrophilicity upon UV irradiation. Surprisingly, Figure 6 shows that this trend is exactly the opposite; the larger the t_{dep} value, the lesser the tunability (i.e., small ΔWCA) for both K = 1.21 and 20 μS/cm. For K = 1.21 μS/cm with numerous beads, as shown in Figure 6a, the hydrophobicity of the nanofibers was substantially reduced with increasing t_{dep}, because of the excessive beads (which gives nonuniform fibers). In addition, hydrophilicity began to dominate with the excessive titania nanoparticles, as confirmed by Figure 7, indicating the increasing titanium content with t_{dep}. As a result, WCAs with t_{dep} = 10 and 15 min were relatively low and their WCA variances were small upon UV irradiation. Only the mat with t_{dep} = 5 min seemed to maintain its tunability as its WCA varied from 93° ± 4° to 40° ± 3° after t_{UV} = 60 min. For K = 20.0 μS/cm, from Figure 6b, initial hydrophobicity was retained because of the disappearance of the beads; the air trapped in the pores between the nanofibers (see Figures 3a−c) managed to yield a similar hydrophobic surface in the WCA range of ∼130°−140°. However, with increasing t_{UV}, the mats coated for $t_{dep} \geq$ 10 min did not seem to have efficient tunability as their WCA variances remained within ΔWCA value of < 20°. Only the mat coated for t_{dep} = 5 min yielded tunability between hydrophilicty and hydrophobicity as the WCA changed from 140° ± 3° to 26° ± 3° (ΔWCA ≈ 115°). This tunability for t_{dep} = 5 min was possible not only because of

the sufficient and uniform air-pockets from the nanofibers, but also because of the sufficient titanium content, as shown by the EDX data from Figure 7. This result suggests that there is an optimal deposition time that yields the optimal mixture of nanofibers and titania nanoparticles to give the targeted tunability between hydrophobicity and hydrophilicity.

Table 1 compares the various methods used for the fabrication of hydrophobic−hydrophlilic tunable films. The fabrication time of our film was 5 min, which was significantly shorter than the fabrication time required by other methods (i.e., 8 h or 2 days). In addition, even under the weakest UV intensity (I = 0.6 W/cm^2), our films yielded a ΔWCA value of 115,° which, by far, indicated the most efficient tunability among the cases, compared in Table 1. Furthermore, this rapid coating process within 5 min fabrication time by electrospraying and electrospinning provided an important route to the realization of low-cost, high- performance, tunable films for antisticking and self-cleaning applications.

4. CONCLUSION

To obtain a functional mat with tunable wettability, a novel three-dimensional (3D) surface structure was utilized to incorporate titania nanoparticles between polystyrene nanofibers. The low surface energy of the polystyrene (PS) nanofibers and the photocatalytic property by the titania nanoparticles provided efficient switching between superhydrophobicity to hydrophilicity for the PS−titania nanocomposite mat. As a result, the maximum limit and the gradual transient of the water contact angle (WCA), as a function of ultraviolet (UV) light illumination time, were successfully obtained. Furthermore, the effects of fabrication parameters, such as the cylinder rotation speed, deposition time, and electrical conductivity of the spinning solution, were also investigated. High electrical conductivity of the spinning solution resulted in bead-free PS nanofibers, which are desirable for retaining hydrophobicity. The optimal rotation speed was ∼300 rpm for the K = 20 μS/cm case, even though its effect did not seem as important as the other parameters. The deposition time (t_{dep}) was an important factor determining the optimal mixture of PS nanofibers and titania nanoparticles. We conclude that a PS−titania composite fabricated by electrospraying and electrospinning is an ideal material for industrial applications that require switchable wettability between hydrophobicity and hydrophilicity.

AUTHOR INFORMATION

Corresponding Author

*Tel.: 82-2-3290-3376. Fax: 82-2-926-9290. E-mail: skyoon@korea.ac.kr.

Notes

The authors declare no competing financial interest.

ACKNOWLEDGMENTS

This study was supported by a grant from the cooperative R&D Program (No. B551179-08-03-00) funded by the Korea Research Council Industrial Science and Technology, Republic of Korea. This research was also supported by the Converging Research Center Program through the Ministry of Education, Science and Technology (No. 2010K000969 and Nos. NRF-2012029433, NRF-2012-0001169, and NRF-2010-0010217).

REFERENCES

(1) Bhardwaj, N.; Kundu, S. C. *Biotechnol. Adv.* **2010**, *28*, 325−347.
(2) Reneker, D. H.; Yarin, A. L. *Polymer* **2008**, *49*, 2387−2425.
(3) Burger, C.; Hsiao, B. S.; Chu, B. *Annu. Rev. Mater. Res.* **2006**, *36*, 333−368.
(4) Nuraje, N.; Khan, W. S.; Lei, Y.; Ceylan, M.; Asmatulu, R. *J. Mater. Chem. A* **2013**, *1*, 1929−1946.
(5) Li, X. M.; Reinhoudt, D.; Crego-Calama, M. *Chem. Soc. Rev.* **2007**, *36*, 1350−1368.
(6) Liu, Y.; Tang, J.; Wang, R.; Lu, H.; Li, L.; Kong, Y.; Qi, K.; Xin, J. *J. Mater. Chem.* **2006**, *17*, 1071−1078.
(7) Shi, F.; Niu, J.; Liu, J.; Liu, F.; Wang, Z.; Feng, X. Q.; Zhang, X. *Adv. Mater. Processes* **2007**, *19*, 2257−2261.
(8) Barthlott, W.; Neinhuis, C. *Planta* **1997**, *202*, 1−8.
(9) Wang, R.; Hashimoto, K.; Fujishima, A.; Chikuni, M.; Kojima, E.; Kitamura, A.; Shimohigoshi, M.; Watanabe, T. *Nature* **1997**, *388*, 431−432.
(10) Xia, F.; Feng, L.; Wang, S.; Sun, T.; Song, W.; Jiang, W.; Jiang, L. *Adv. Mater.* **2006**, *18*, 432−436.
(11) Xin, B.; Hao, J. *Chem. Soc. Rev.* **2010**, *39*, 469−782.
(12) Lau, K. K. S.; Bico, J.; Teo, K. B. K.; Chhowalla, M.; Amaratunga, G. A. J.; Milne, W. I.; McKinley, G. H.; Gleason, K. K. *Nano Lett.* **2003**, *3*, 1701−1705.
(13) Chen, X.; Wu, J.; Ma, R.; Hua, M.; Koratkar, N.; Yao, S.; Wang, Z. *Adv. Funct. Mater.* **2011**, *21*, 4617−4623.
(14) Xiao, W.; Huang, Z.; He, Z. *Appl. Phys. Lett.* **2006**, *89*, 083101.
(15) Kim, T. G.; Park, T. G. *Biotechnol. Prog.* **2008**, *22*, 1108−1113.
(16) Liang, D.; Hsiao, B. S.; Chu, B. *Adv. Drug Delivery Rev.* **2007**, *59*, 1392−1412.
(17) Chu, B.; Liang, D.; Hadjiargyrou, M.; Hsiao, B. S. *J. Phys.: Condens. Matter* **2006**, *18*, S2513.
(18) Ng, L. Y.; Mohammad, A. W.; Leo, C. P.; Hilal, N. *Desalination* **2013**, *308*, 15−33.
(19) Alf, M. E.; Asatekin, A.; Barr, M. C.; Baxamusa, S. H.; Chelawat, H.; Ozaydin-Ince, G.; Petruczok, C. D.; Sreenivasan, R.; Tenhaeff, W. E.; Trujillo, N. J. *Adv. Mater.* **2010**, *22*, 1993−2027.
(20) Dai, Y. A.; Chang, H. C.; Lai, K. Y.; Lin, C. A.; Chung, R. J.; Lin, G. R.; He, J. H. *J. Mater. Chem.* **2010**, *20*, 10924−10930.
(21) Kim, B. S.; Shin, S.; Shin, S. J.; Kim, K. M.; Cho, H. H. *Langmuir* **2011**, *27*, 10148−10156.
(22) Tsougeni, K.; Tserepi, A.; Boulousis, G.; Constantoudis, V.; Gogolides, E. *Plasma Processes Polym.* **2007**, *4*, 398−405.
(23) Deitzel, J.; Kleinmeyer, J.; Harris, D.; Beck Tan, N. *Polymer* **2001**, *42*, 261−272.
(24) Hellmann, C.; Belardi, J.; Dersch, R.; Greiner, A.; Wendorff, J.; Bahnmueller, S. *Polymer* **2009**, *50*, 1197−1205.
(25) He, X.; Arsat, R.; Sadek, A.; Wlodarski, W.; Kalantar-zadeh, K.; Li, J. *Sens. Actuators B* **2010**, *145*, 674−679.
(26) Lu, X.; Li, L.; Zhang, W.; Wang, C. *Nanotechnology* **2005**, *16*, 2233.
(27) Singh, A.; Steely, L.; Allcock, H. R. *Langmuir* **2005**, *21*, 11604−11607.
(28) Miyauchi, Y.; Ding, B.; Shiratori, S. *Nanotechnology* **2006**, *17*, 5151.
(29) Seidi, A.; Ramalingam, M.; Elloumi-Hannachi, I.; Ostrovidov, S.; Khademhosseini, A. *Acta Biomater.* **2011**, *7*, 1441−1451.
(30) Coutinho, D.; Costa, P.; Neves, N.; Gomes, M. E.; Reis, R. L. *Tissue Eng.* **2011**, 3−29.
(31) Song, M. Y.; Ihn, K. J.; Jo, S. M.; Kim, D. Y. *Nanotechnology* **2004**, *15*, 1861.
(32) Yang, D.; Liu, X.; Jin, Y.; Zhu, Y.; Zeng, D.; Jiang, X.; Ma, H. *Biomacromolecules* **2009**, *10*, 3335−3340.
(33) Wu, D.; Han, D.; Steckl, A. J. *ACS Appl. Mater. Interfaces* **2009**, *2*, 252−258.
(34) Lin, T.; Wang, X. *Int. J. Nanotechnol.* **2009**, *6*, 579−598.
(35) Chen, S.; Hou, H.; Harnisch, F.; Patil, S. A.; Carmona-Martinez, A. A.; Agarwal, S.; Zhang, Y.; Sinha-Ray, S.; Yarin, A. L.; Greiner, A. *Energy Environ. Sci.* **2011**, *4*, 1417−1421.

(36) Gopal, R.; Kaur, S.; Ma, Z.; Chan, C.; Ramakrishna, S.; Matsuura, T. *J. Membr. Sci.* **2006**, *281*, 581−586.
(37) Zheng, J.; He, A.; Li, J.; Xu, J.; Han, C. C. *Polymer* **2006**, *47*, 7095−7102.
(38) Guan, K. *Surf. Coat. Technol.* **2005**, *191*, 155−160.
(39) Asmatulu, R.; Ceylan, M.; Nuraje, N. *Langmuir* **2010**, *27*, 504−507.
(40) Jin, M.; Zhang, X.; Emeline, A. V.; Numata, T.; Murakami, T.; Fujishima, A. *Surf. Coat. Technol.* **2008**, *202*, 1364−1370.
(41) Rayleigh, L. *Proc. London Math. Soc.* **1878**, *10*, 4−13.
(42) Reneker, D. H.; Yarin, A. L.; Zussman, E.; Xu, H. *Adv. Appl. Mech.* **2006**, *41*, 43−195.
(43) Fallahi, D.; Rafizadeh, M.; Mohammadi, N.; Vahidi, B. *Polym. Int.* **2008**, *57*, 1363−1368.
(44) Lin, T.; Wang, H.; Wang, H.; Wang, X. *Nanotechnology* **2004**, *15*, 1375.
(45) Uyar, T.; Besenbacher, F. *Polymer* **2008**, *49*, 5336−5343.
(46) Ma, M.; Mao, Y.; Gupta, M.; Gleason, K. K.; Rutledge, G. C. *Macromolecules* **2005**, *38*, 9742−9748.
(47) Zhu, Y.; Zhang, J.; Zheng, Y.; Huang, Z.; Feng, L.; Jiang, L. *Adv. Funct. Mater.* **2006**, *16*, 568−574.
(48) Han, D.; Steckl, A. J. *Langmuir* **2009**, *25*, 9454−9462.
(49) Tu, C. W.; Tsai, C. H.; Wang, C. F.; Kuo, S. W.; Chang, F. C. *Macromol. Rapid Commun.* **2007**, *28*, 2262−2266.
(50) Stevens, N.; Priest, C. I.; Sedev, R.; Ralston, J. *Langmuir* **2003**, *19*, 3272−3275.
(51) Boinovich, L.; Emelyanenko, A. M.; Pashinin, A. S. *ACS Appl. Mater. Interfaces* **2010**, *2*, 1754−1758.
(52) Ivanova, N. A.; Zaretskaya, A. K. *Appl. Surf. Sci.* **2010**, *257*, 1800−1803.
(53) Boinovich, L. B.; Emelyanenko, A. M.; Pashinin, A. S.; Lee, C. H.; Drelich, J.; Yap, Y. K. *Langmuir* **2012**, *28*, 1206−1216.
(54) Lee, H. Y.; Park, Y. H.; Ko, K. H. *Langmuir* **2000**, *16*, 7289−7293.
(55) Zhang, X.; Jin, M.; Liu, Z.; Tryk, D. A.; Nishimoto, S.; Murakami, T.; Fujishima, A. *J. Phys. Chem. C* **2007**, *111*, 14521−14529.